Robust estimation of dynamic cerebrovascular reactivity using breath-holding fMRI: application in diabetes and hypertension

Nuwan D. Nanayakkara[1], Liesel-Ann Meusel[1], Nicole D. Anderson[1,2], J. Jean Chen[1,3,4]

[1]Rotman Research Institute, Baycrest Academy for Research and Education; [2]Departments of Psychology and Psychiatry, University of Toronto; [3]Department of Medical Biophysics, University of Toronto; [2]Department of Biomedical Engineering, University of Toronto

Abstract

Breath-holding (BH) tasks during functional magnetic resonance imaging (fMRI) acquisitions are gaining popularity for non-invasive mapping of carbon-dioxide (CO_2) driven cerebrovascular reactivity (CVR), which is a valuable clinical marker of vascular function. However, compliance to BH tasks is often unclear, and the ability to record end-tidal CO_2 often limited, rendering the optimal analysis of BH fMRI data a challenge. In this work, we demonstrate an adaptive data-driven approach for estimating CVR from BH fMRI data that minimizes errors due to subject non-compliance and regional CVR time delay variability. Building on previous work, we propose a frequency-domain-based approach for CVR estimation without the need for end-tidal CO_2 ($PETCO_2$) recordings. CVR amplitude is estimated in units of %ΔBOLD directly from the data-driven BH frequency. Serious deviations from the designed task paradigm were suppressed and thus did not bias the estimated CVR values. We demonstrate our method in detecting regional CVR amplitude and time-lag differences in a group of 56 individuals, consisting of healthy (CTL), hypertensive (HT) and diabetic-hypertensive (DM+HT) groups of similar ages and sex ratios. The CVR amplitude was lowest in HT+DM, and HT had a lower CVR amplitude than CTL regionally but the voxelwise comparison did not yield statistical significance. Notably, we demonstrate that the voxelwise CVR time delay estimated in Fourier domain is a more sensitive marker of vascular dysfunction than CVR amplitude. While HT+DM seems to confer longer CVR delays, HT seems to confer shorter delays than CTL. These are the first MRI-based observations of CVR time delay differences between diabetic-hypertensive patients and healthy controls. These results demonstrate the feasibility of extracting CVR amplitude and CVR time delay using BH challenges without $PETCO_2$ recordings, and the unique clinical value of CVR time-delay information.

1. Introduction

Cerebrovascular reactivity (CVR) is a useful metric to assess how well the vasculature dilates or constricts in response to various stimuli. CVR is sensitive to various pathological conditions making it a potential biomarker [Giordani et al., 2014; Iranmahboob et al., 2016; Ivankovic et al., 2013; Liu et al., 2021; Petrica et al., 2007; Yazdani et al., 2020]. CVR also exhibits spatiotemporal variations even in the healthy brain due to regional differences in the cerebral vasculature [Bright et al., 2009; Lipp et al., 2015; Thomas et al., 2013]. Measurement of changes in CBF in response to a vasoactive stimulus is used to estimate CVR with the help of different neuroimaging methods such as transcranial Doppler ultrasound (TCD) [Kleiser and Widder, 1992], single-photon emission computed tomography (SPECT), and positron emission tomography (PET) [Ogasawara et al., 2003]. However, functional magnetic resonance imaging (fMRI) has been widely adopted for CVR measurements due to its ability to provide non-invasive whole-brain CVR estimation at an acceptable spatial and temporal resolution [Pinto et al., 2020; Urback et al., 2017]. The BOLD contrast is the most common for use in CVR mapping using MRI as it depends on the relative CBF changes in response to a vasoactive stimulus [Chen and Pike, 2010; Hauser et al., 2019; Mandell et al., 2008]. The advantages of direct measurement of CBF using non-invasive arterial spin labeling (ASL) perfusion imaging have also been demonstrated [Halani et al., 2015; Zhao et al., 2021], but the use of ASL is less frequent due to technical and availability constraints [Alsop et al., 2015; Heijtel et al., 2014].

Various vascular stimuli have been used to enable CVR mapping. The inhalation of air containing elevated CO_2 content has been used frequently in CVR mapping [Liu et al., 2017b; Mark et al., 2010; Wise et al., 2007]. However, inhalation-based methods typically require complex experimental setups including breathing masks and are often not well tolerated by vulnerable groups such as children and the elderly [Spano et al., 2013]. Breath-hold (BH) tasks involve minimal setup and have been suggested as a robust alternative to gas challenges [Bright and Murphy, 2013; Lipp et al., 2015; Pinto et al., 2020; Urback et al., 2017]. BH tasks have been well tolerated by less cooperative subjects of vulnerable groups [Dlamini et al., 2018; Raut et al., 2016] and have been successfully applied in clinical studies [Haight et al., 2015; Iranmahboob et al., 2016; Raut et al., 2016; Tchistiakova et al., 2014]. A typical BH task follows a protocol consisting of a block design with alternating periods of normal breathing and breath holding for a simple reproducible voluntary breathing modulation task [Lipp et al., 2015; Peng et al., 2020; Pinto et al., 2016]. Nonetheless, well-known caveats of BH methods include the greater need for participant cooperation [Urback et al., 2017; Wu et al., 2015] and the unavailability of expired gas measurements during the BH periods, especially as a given BH task pattern across multiple subjects do not necessarily produce similar increases in CO_2 partial pressure values in the blood [Urback et al., 2017] To help address this cause of uncertainty, some studies have incorporated measurement of end-tidal carbon dioxide partial pressure ($PETCO_2$) using a mask or nasal cannula [Bright and Murphy, 2013; Pinto et al., 2016; Sousa et al., 2014]. A short BH period of 6 s can result in hypercapnia [Abbott et al., 2005] while

the spatial extent of the significant BOLD response reaches a plateau at a BH length of around 20 s [Liu et al., 2002]. Many studies have reported a BH length of 15 s for successful estimation of CVR from BOLD data [Chang et al., 2008; Geranmayeh et al., 2015; Lipp et al., 2015; Tchistiakova et al., 2014; Urback et al., 2018]. With careful analysis, the performances of BH can be comparable to those involving gas manipulation techniques [Kannurpatti and Biswal, 2008; Liu et al., 2017a; Tancredi and Hoge, 2013; Wu et al., 2015]. However, at the CVR estimation step, uncertainties in subject compliance can present major data-analysis challenges, especially when $PETCO_2$ recordings are unavailable.

Model-driven approaches such as the general linear model (GLM) have been employed to estimate CVR from BOLD responses to a BH task, whereby the BH paradigm is modelled as a boxcar [Biswal et al., 2007; Kastrup et al., 1999] or ramp function convolved with a hemodynamic response function (HRF) to approximate linear BOLD signal increases [Bright and Murphy, 2013]. Additional temporal derivatives of the HRF are required to account for the longer delays in respiratory responses to appear in the BOLD signal [Jahanian et al., 2017; Murphy et al., 2011]. The GLM model-driven approaches use a single fixed time lag in HRF to fully describe the BOLD signal across the whole brain. However, different brain regions exhibit different temporal CVR dynamics, both in healthy subjects and in patients [Chang et al., 2008; Geranmayeh et al., 2015; Magon et al., 2009; Pinto et al., 2016; Stringer et al., 2021]. Previous studies incorporating cross-correlations to estimate optimal time lags of the BOLD response have demonstrated substantial response-time variations across the brain [Chang et al., 2008; Geranmayeh et al., 2015]. The global BOLD time series has also been used in some studies as a reference to estimate the CVR time delay, ignoring the regional variations [Geranmayeh et al., 2015]. Iterative GLM fitting with shifted regressors [Geranmayeh et al., 2015; Moia et al., 2021; Murphy et al., 2011; Niftrik et al., 2016; Pinto et al., 2016] has also been successfully used in previous studies to estimate voxelwise CVR time delay. However, it is evident that GLM methods work best when $PETCO_2$ recordings are available as input, allowing both inter-subject variations in BH compliance and in respiratory physiology to be accounted for [Birn et al., 2008; Bright and Murphy, 2013; Lipp et al., 2015; Murphy et al., 2011]. Moreover, the canonical hemodynamic response function is derived using the BOLD response to neuronal activity and not CO_2.

We propose a novel approach for estimating the amplitude and timing of the BH BOLD response without modelling or correlation with other signals (e.g. PETCO2). Our approach makes use of the Fourier representation of the spectrum of BOLD data, as it has been found that the BH CVR response can be successfully approximated as a sinusoidal signal by assuming the BH task is approximately symmetrical (equivalent BH and baseline periods), even if it is not [Lipp et al., 2015; Murphy et al., 2011]. This sinusoidal approach was shown to outperform the use of an HRF-based regressor (the $PETCO_2$ trace convolved with the HRF [Niftrik et al., 2016]), prompting us to estimate CVR in the Fourier domain. Indeed, in the Fourier-series-based regression approach by Pinto et al., BH designs that deviate further

from symmetry can be addressed by adding higher harmonics to the Fourier series [Pinto et al., 2016]. On the other hand, our data-driven Fourier-based approach does not require regressors but instead detects and accounts for deviations from task designs directly from the BOLD fMRI data. In this study, we used a typical BH task design similar to the studies mentioned earlier. We demonstrate our method by assessing differences in CVR amplitude and time delay among patients with hypertension (HT), hypertension-plus-type-2 diabetes (HT+DM), and age-matched controls (CTL).

2. Methods

2.1. Study participants

Older adults of ages 65-85 were recruited and placed in control (CTL), hypertension (HT), or hypertension-plus-type-2 diabetes (HT+DM) groups on the basis of screening measures. Participants were excluded from the study if they met any of the following criteria: (1) a score ≤ 31 on the Telephone Interview for Cognitive Status – modified version [Welsh et al., 1993] in order to exclude participants with possible dementia; (2) the use of insulin to treat DM; (3) the presence of DM complications, based on self-report, including clinically significant gastroparesis, retinopathy, nephropathy, neuropathy, hepatic disease, or a recent coronary heart disease event as determined by a physician; (4) other significant medical or psychiatric disorders affecting cognitive function, such as stroke (self-report or evidence from structural scans) and major depressive disorder; (5) current or recent use of central nervous system-active medications, including those for the treatment of depression, sleep disorders, and migraine headaches; (6) major inflammatory disorders, heart failure, and chronic lung disease; or (7) hormone replacement therapy in female participants. The included participants were screened to ensure group status as listed below:

- CTL: Participants had a mean systolic BP ≤ 140 mmHg, a mean diastolic BP ≤ 90 mmHg, no history of antihypertensive medication use, and a fasting glucose level (FGL) ≤ 6.1 mmol/L.
- HT: Participants were using antihypertensive medication under physician prescription for a minimum of two years, with current blood pressure within a normal or HT range and limited to those who were using long-acting antihypertensive medications (e.g., ACEIs, angiotensin II receptor blockers, diuretics) in order to capture the most commonly prescribed medications.
- HT+DM: Participants had a physician diagnosis of type 2 DM for a duration of at least two years, were controlling their DM through diet or hypoglycemic medication alone, and were free of major DM complications as defined in the exclusion criteria, in addition to the criteria for the HT.

All selected participants completed a brief medical questionnaire, which included questions about the use and duration of all medications and the duration of HT and DM. Participants provided a fasting blood sample for measurement of hematocrit, lipid profile (triacylglycerides [TG], total cholesterol [TC], low-density lipoprotein [LDL], and high-density lipoprotein [HDL]), CRP, glucose, insulin, and HbA1c. Blood pressure, weight, height, and waist circumference were also measured. These measurements were

followed by a practice session of the breath hold task in an MRI simulator to ensure that the participant was comfortable with the fMRI scanning protocol. Participants were asked to continue their usual diet, medications, and activity level for the duration of their involvement in the study. Available data from 56 participants (CTL:21, HT: 23, and HT+DM: 12) were preprocessed as described in Section 2.3. Data from seven participants (CTL:3, HT:3, and HT+DM:1) were removed from analysis due to excessive head-motion artifacts larger than 1^{o} rotation and 1 mm translation as detected by FSL motion correction. This study consisted of remaining data from 49 participants (CTL: 18, HT: 20, and HT+DM: 11) with mean ages of 70.2 ± 3.3, 71.9 ± 4.7, and 71.7 ± 3.6 years, and male/female ratios of 1.25, 0.43 and 0.57, respectively.

2.2. Data acquisition

Each participant followed a set of 6 repetitions of a 30 s resting and 2 s exhale followed by a 15 s BH guided by visual clues (total duration, T = 47 s) during a dual-echo pCASL fMRI image acquisition session on a Siemens Trio 3T system (T2*-weighted echo-planar imaging, FOV = 220 mm, acquisition matrix = 220 x 220, voxel size = 3.4 x 3.4 x 6.0 mm, bandwidth = 2790 Hz/Pixel, TE1/TE2/TR = 9.1/25/4000 ms, flip angle = 90 degrees, slices = 16, averages = 1, concatenations = 1, scan duration = 5:24). The data associated with the second TE were used to compute the BOLD time series. Respiratory bellows were recorded using the scanner's built-in belt. A T1 anatomical scan (FOV = 256 mm, acquisition matrix = 192 x 256, voxel size = 1.0 mm^3, bandwidth = 200 Hz/Pixel, TI/TE/TR = 1100/2.63/2000 ms, flip angle = 9 degrees, slices = 160, averages = 1, concatenations = 1, scan duration = 6:26) was acquired for anatomical reference and tissue segmentation.

2.3. Preprocessing

The dual-echo pCASL time series data were preprocessed using FSL [Jenkinson et al., 2012; Smith et al., 2004] and AFNI [Cox, 1996; Cox and Hyde, 1997] tools. Slice timing correction using *slicetimer* in FSL was applied to correct for sampling offsets inherent in slice-wise EPI acquisition sequences. The BOLD data in the dual-echo pCASL time series were isolated from the full pCASL time series and separated into odd and even time frames. Both of these time series were separately corrected for subject motion using the *mcflirt* and registered into MNI space using *flirt*. AFNI's *3dretroicor* was used to generate BOLD data that were corrected for noise associated with physiological motion (i.e., heartbeat, respiration). Neighbouring control and tag frames were averaged in a sliding-window manner to produce 78 frames of BOLD data, which were then high-pass filtered to remove low-frequency noise from the data with a 0.01 Hz cut-off frequency, resulting in the "preprocessed BOLD signal".

2.4. Data-driven CVR estimation

CVR estimation was performed on the preprocessed BOLD data using our robust data-driven pipeline shown in **Figure 1**. The BOLD data was first normalized by the mean of the first 8 frames of the series corresponding to the baseline before the first BH period. The time series data was then converted to %ΔBOLD by voxelwise demeaning. As described earlier, the identification of the BH frequency (BHF) can be hampered by variations in task compliance as well as in participant physiology. Thus, the identification of the BHF in our pipeline undergoes a two-step process to ensure flexibility and robustness. First, we identified the BH task paradigm used in the study that can be considered as a repetitive signal of period T = 47 s, corresponding to a fundamental BHF of $\frac{1}{T}$ (0.0213 Hz). The voxelwise BOLD signal was passed through a bandpass filter of cut-off frequencies $\left[\frac{1}{(T+0.33T)}, \frac{1}{(T-0.33T)}\right] = [0.0158, 0.0323]$ Hz, corresponding to *T*±*T/3*. The pipeline finds the BHF from the BOLD data spectrum within this frequency range, such that the BHF can deviate slightly from the nominal frequency due to variations in subject compliance with the task design, but is not allowed to deviate too far away from the expected task frequency to ensure robustness against noise. Second, the pipeline finds the BHF corresponding to the maximum amplitude of the Fourier spectrum of the BOLD signal at each cortical voxel. Lastly, for the grey matter (GM) of each data set, a histogram is constructed using the voxel-wise BHF, and the BHF found at the peak occurrence is chosen as the dominant BHF for that data set. This second step further constrains the BHF to maximize inter-regional comparability, assuming that variations in respiratory physiology contribute to inter-subject but not within-subject inter-regional CVR differences. That is, the dominant BHF can vary between participants but not between brain regions.

When a reference signal is available, the voxelwise phase (ϕ_s) of the CVR at BHF relative to a reference signal at the same frequency can be used to compute a response lag for the CVR response. One such reference is the respiratory belt recording, which was used in this study. The envelope of the respiratory signal was extracted from the recording, which also allowed us to verify each subject's compliance with the BH task. The phase (ϕ_r) of the de-meaned respiratory belt signal envelope Fourier spectrum at the BHF was selected as the reference for CVR time delay, calculations as

$$\text{CVR time delay} = \frac{(\phi_s - \phi_r)}{2\pi \times BHF}$$

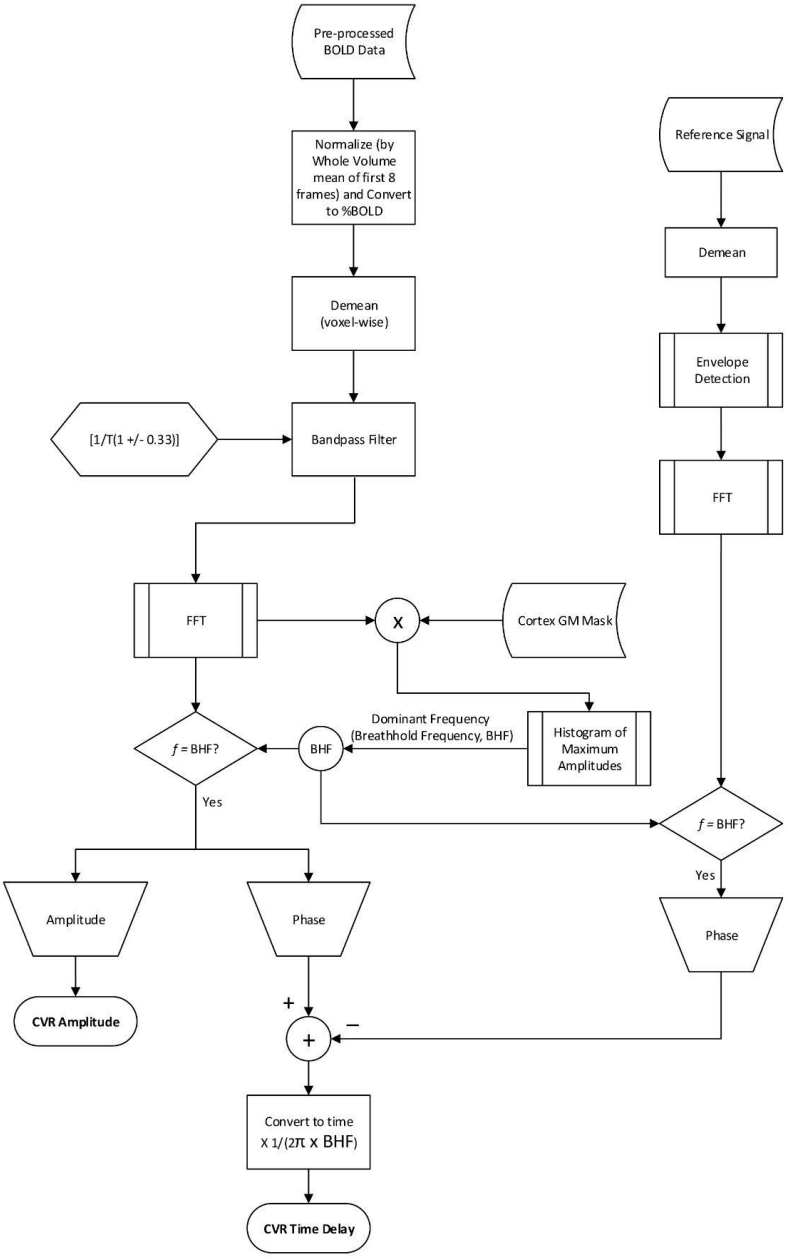

Figure 1. Signal processing pipeline. The normalized and demeaned %ΔBOLD data were bandpass filtered to retain signals around the targeted BH frequency (BHF). The dominant frequency of the filtered signal in the cortex was selected as the BHF. The amplitude of the spectrum of each voxel the BHF was selected as the CVR amplitude. The CVR response time of each voxel was calculated relative to the BH task extracted at the BHF using the envelope of the respiratory belt signal.

2.5. Statistical analysis

We also computed the Framingham Risk Score (FRS) [Wilson et al., 1998] and Diabetes Epidemiology: Collaborative Analysis of Diagnostic Criteria in Europe (DECODE) scores [Balkau et al., 2004]. Differences in demographics and physiological measurements across groups, including the FRS and DECODE metrics, were detected by ordinary one-way ANOVA corrected for multiple comparisons by controlling the false discovery rate using the Benjamini-Hochberg procedure.

The CVR amplitude and time delay were compared voxelwise and region-wise across the three groups (namely CTL, HT, and HT+DM). The GLM approach [Winkler et al., 2014] was used for the voxelwise comparison followed by multiple comparisons correction via threshold-free cluster enhancement [Smith and Nichols, 2009]. Brain parcellations generated by nonlinear spatial registration of T1-anatomical scan to the default GCA atlas in FreeSurfer (Version 6.0.1, available at surfer.nmr.mgh.harvard.edu) were used to calculate mean CVR amplitudes and mean CVR time delays in cortical regions in each group. The mean regional CVR amplitudes were normally distributed in all three groups while the distributions of time delays were not normal when tested using the D'Agostino-Pearson test [D'Agostino and Stephens, 1986] for normality (see supplementary table S1). Two-way ANOVA with multiple comparisons was used to compare the overall means of region-wise (ROI) CVR amplitude, corrected for multiple comparisons by controlling the false discovery rate (Benjamini-Hochberg procedure) between groups. The statistically significant differences detected by Friedman's test were corrected for multiple comparisons by controlling the false discovery rate using the Benjamini-Hochberg procedure for whole group-wise comparison of overall means of CVR time delay. Regional CVR amplitude and time delay were compared seperately in each cortical region of interest (ROI) using the Kruskal-Wallis test corrected for multiple comparisons by controlling the false discovery rate.

3. Results

Figure 2 summarizes the demographics and physiological measurements for participants in the three groups. Participant age was not significantly different across the groups (**Figure 2a).** HT and HT+DM groups did not exhibit significant differences in systolic BP (SBP) compared to CTL (**Figure 2b)**. The HT+DM group showed significantly higher HbA1C and lower LDL cholesterol values compared to the HT and CTL groups (**Figure 2c, d)**. The FRS and DECODE scores were both significantly lower in CTL compared to HT and HT+DM, but only the DECODE score showed a significantly lower score for HT compared to HT+DM (**Figure 2e, f**).

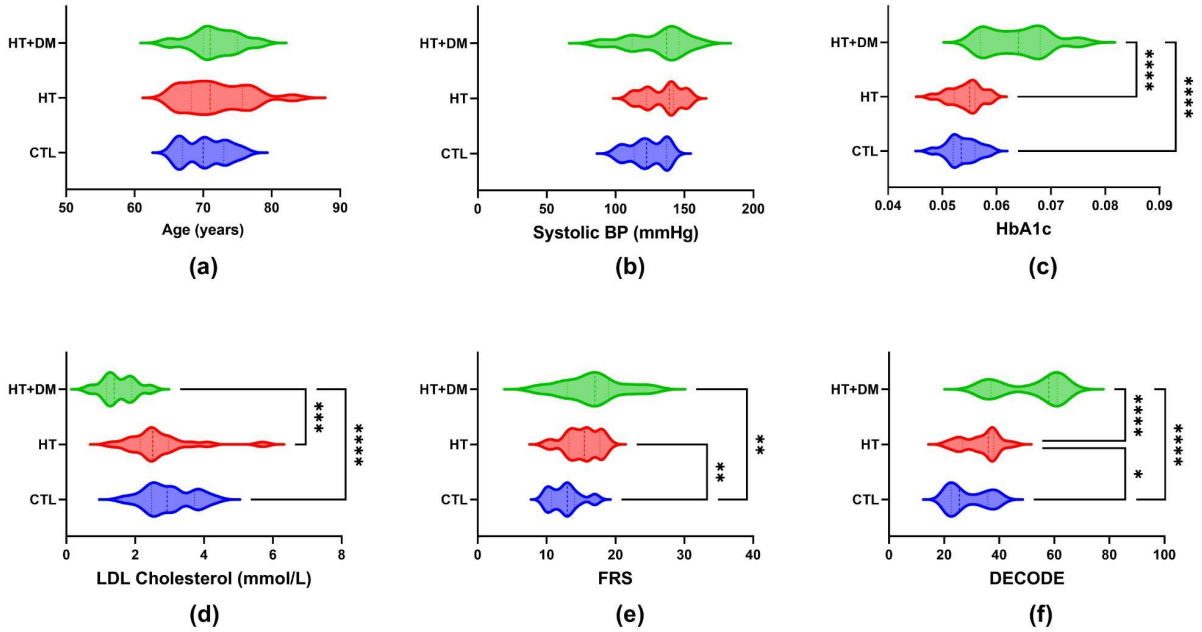

Figure 2. Subject demographics. The mean (a) age, (b) systolic blood pressure, (c) HbA1c values, (d) LDL cholesterol, (e) Framingham Risk Score (FRS), and (f) Diabetes Epidemiology: Collaborative Analysis of Diagnostic Criteria in Europe (DECODE) score for each subject group. The statistically significant differences were detected by ordinary one-way ANOVA corrected for multiple comparisons by controlling the false discovery rate using the Benjamini-Hochberg procedure indicated by * ($q < 0.05$), ** ($q < 0.01$), *** ($q < 0.001$) and **** ($q < 0.0001$).

Shown in **Figure 3** are sample signals from the intermediate steps of the signal processing pipeline for a participant compliant (3a) and a participant non-compliant (3b) to the BH task design. Bandpass filtering suppressed spurious signals outside the targeted BHF range, as in Figure 3a(ii) and 3b(ii). The histograms of maximum amplitudes of the bandpass-filtered BOLD spectra in all cortical voxels are shown in **Figure 3a(i) and 3b(i)** for sample subjects. The peaks of the histograms correspond to the dominant CVR frequencies. In addition, the BOLD signal at the dominant frequency is well-modelled by the sinusoidal approximation and closely follows the respiratory belt signal as shown in **Figure 3a(v) and 3b(v)**, even when the subject performance on the BH task deviated from the task design.

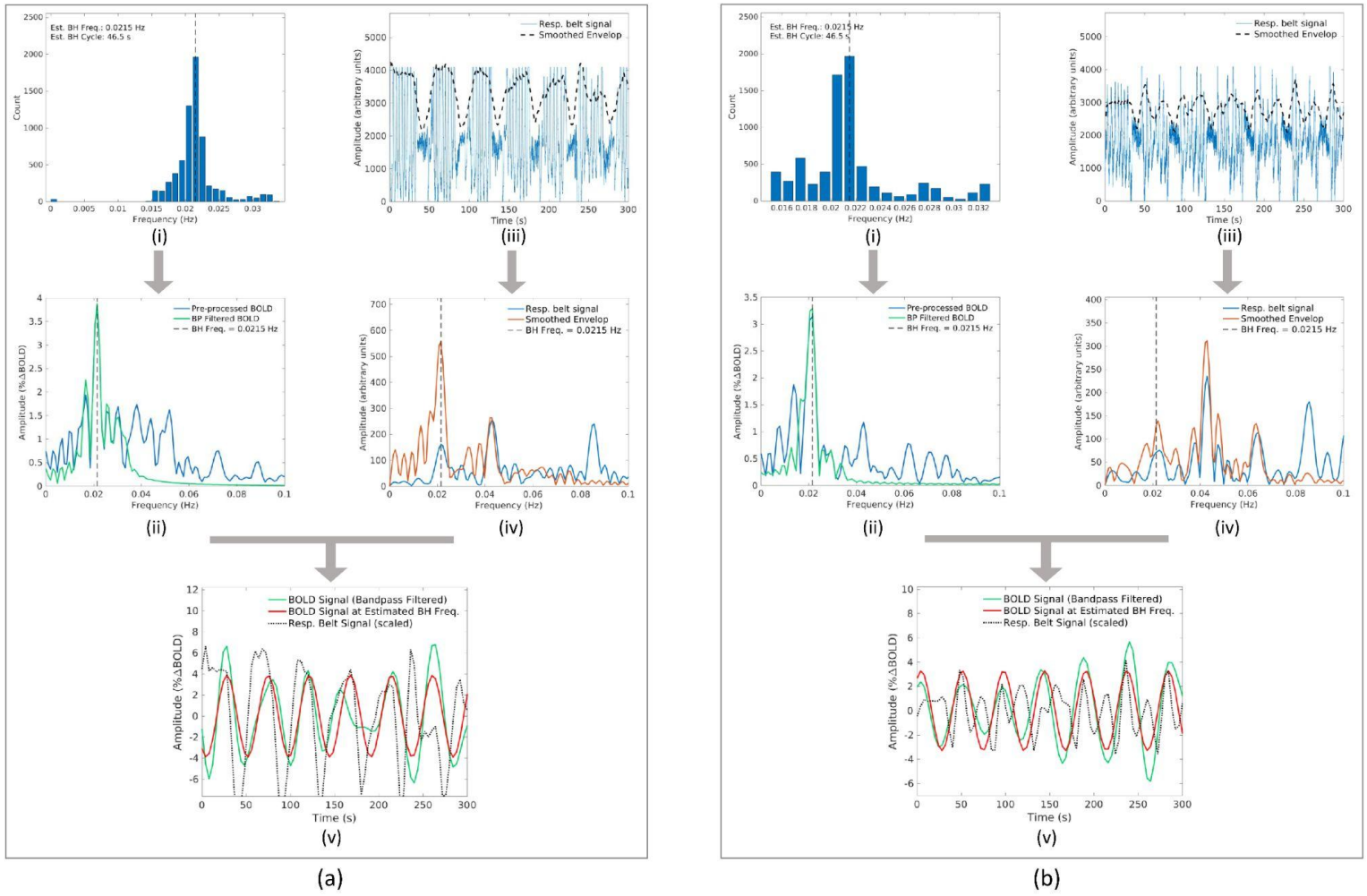

Figure 3. Samples outputs from intermediate signal-processing steps. Samples from the signal processing pipeline for a subject (a) compliant and (b) non-compliant to BH task design. Each includes (i) the histogram of maximum amplitudes at all cortical voxels with corresponding frequencies, (ii) the frequency spectrum of the pre-processed and band-pass filtered BOLD at a sample voxel in the cortex, (iii) the respiratory belt signal with the smoothened envelope, (iv) respective frequency spectrum of the belt signal, and (v) bandpass filtered the BOLD signal, and the estimated CVR response at the BHF at the sample voxel in the cortex.

Figure 3 shows the recorded full respiratory-belt signal and the extracted BH pattern from the smoothed envelope details with corresponding frequency spectrums for a participant who followed the BH task paradigm (**figures 3a(iii)** and **3a(iv)** respectively) and for a participant who was not compliant (**figures 3b(iii)** and **3b(iv)** respectively). As indicated by dashed lines on respective frequency spectrums, the proposed data-driven approach was able to correctly estimate the BHF in both cases avoiding peaks from unexpected frequencies.

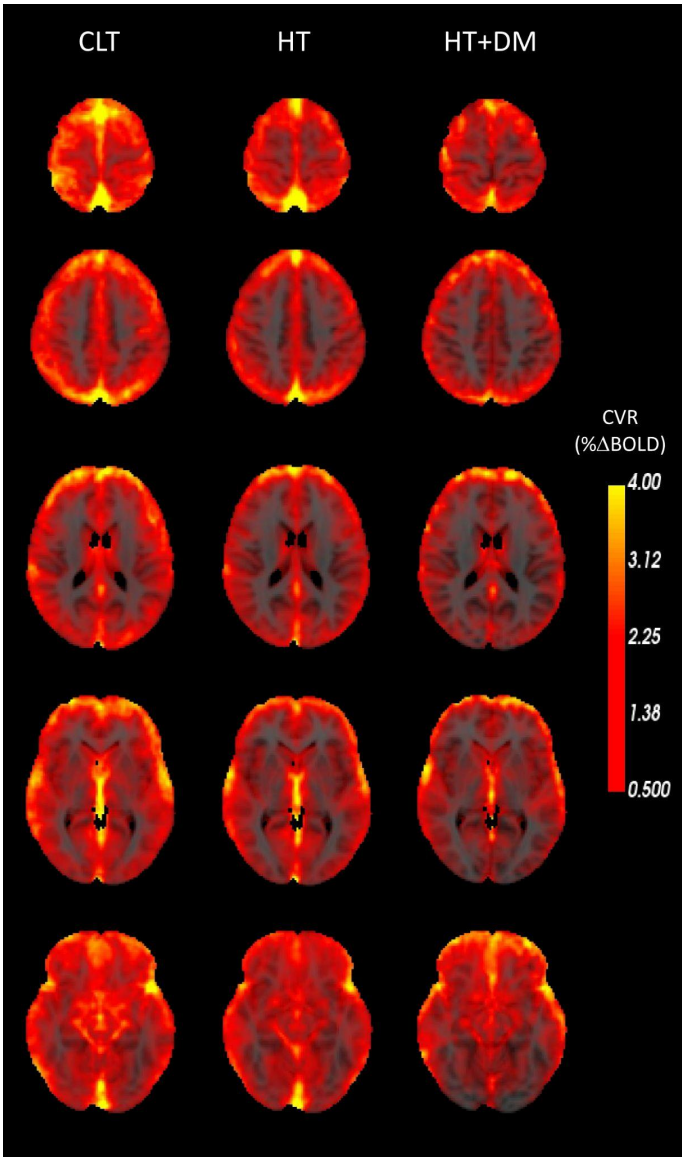

Figure 4. Mean CVR amplitude (%ΔBOLD) for all subjects in each group. The grey matter (GM) regions in the cortex have a higher CVR amplitude than the white-matter (WM) and other areas of the brain. The HT+DM participants showed the lowest CVR amplitudes consistently throughout all brain regions.

Figure 4 shows the mean CVR amplitude maps in each group. GM regions in the cortex generally have a higher CVR amplitude compared to other areas of the brain. The mean CVR amplitude in CTL was significantly higher than both HT and HT+DM across cortical GM and higher in HT compared to HT+DM (see supplementary figure S1a).

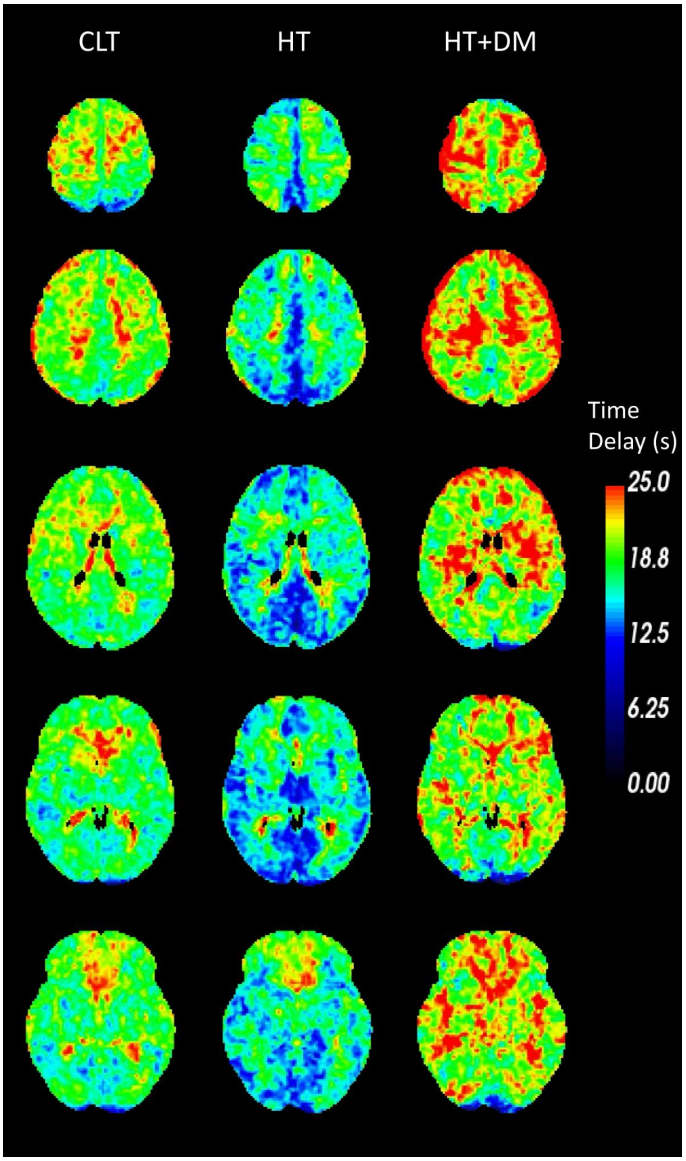

Figure 5. Mean CVR time delay (s) relative to the respiratory belt signal in each group. The GM regions in the cortex have a shorter CVR time delay than the WM and other areas of the brain. The HT group showed the lowest CVR time delay while HT+DM group showed the longest delay.

Figure 5 shows the mean CVR time delay maps in each group. GM regions in the cortex generally have a shorter delay than in other areas of the brain. The mean CVR time delay in HT+DM was significantly

longer than both CTL and HT across cortical GM and longer in CTL compared to HT (see supplementary **figure S1b**).

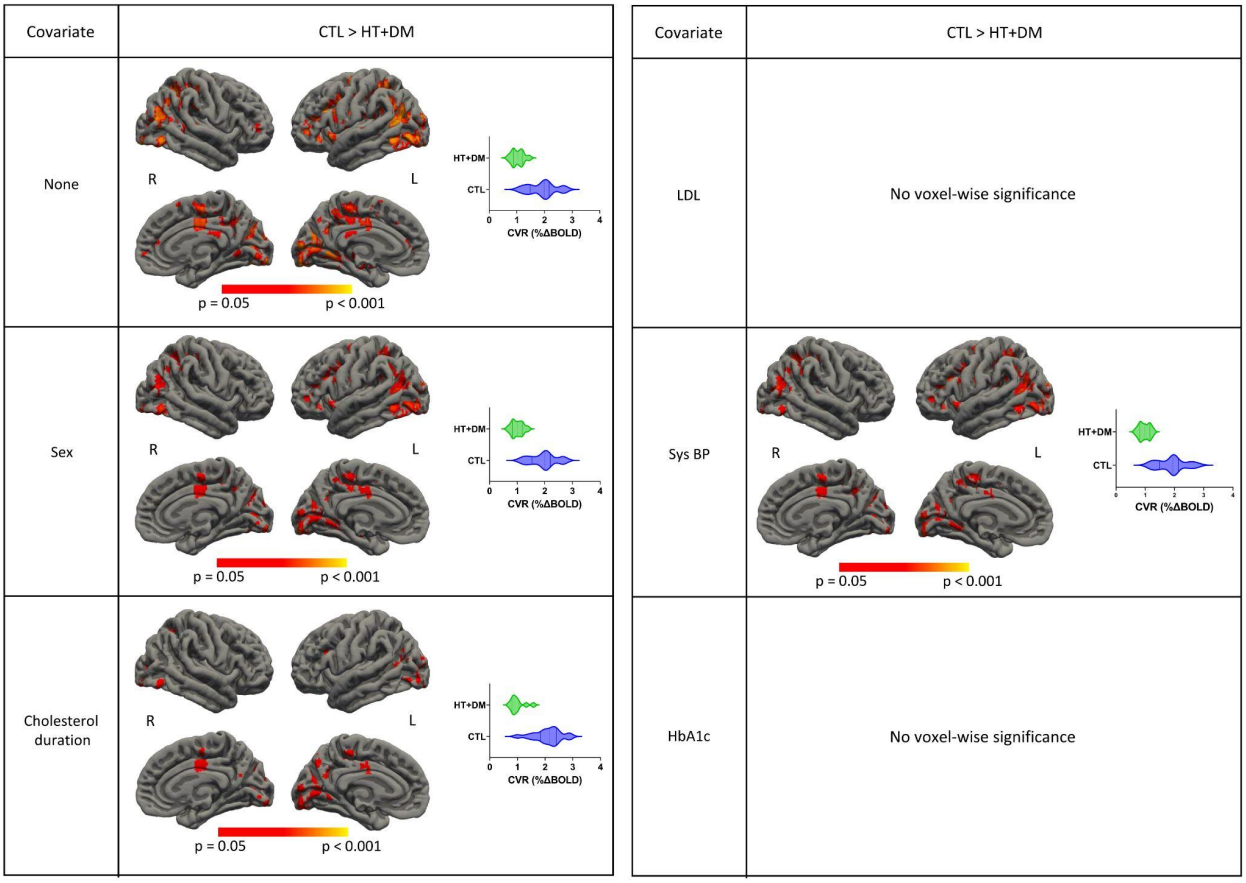

Figure 6. Voxelwise comparisons of CVR amplitudes. The statistical testing on CVR amplitudes of CTL > HT+DM showed significant voxels ($p < 0.05$) for permutation inference for the general linear model after threshold-free cluster enhancement. The significance of differences in most voxels was reduced when controlled for sex, the duration of previously detected hypercholesterolemia, or systolic blood pressure. No statistical significance voxels were detected when controlling for LDL or HbA1c. Significant differences in CVR amplitude were not detected between CTL and HT or between HT and HT+DM.

Figure 6 shows voxels that demonstrate statistically significant differences ($p < 0.05$) where CVR amplitudes in CTL > HT+DM. Most CVR amplitude differences were reduced when controlling for sex, the duration of previously detected hypercholesterolemia, or systolic blood pressure. No statistical significance voxels were detected when controlling for LDL or HbA1c. No significant voxelwise differences in CVR amplitudes were detected between CTL and HT or between HT and HT+DM.

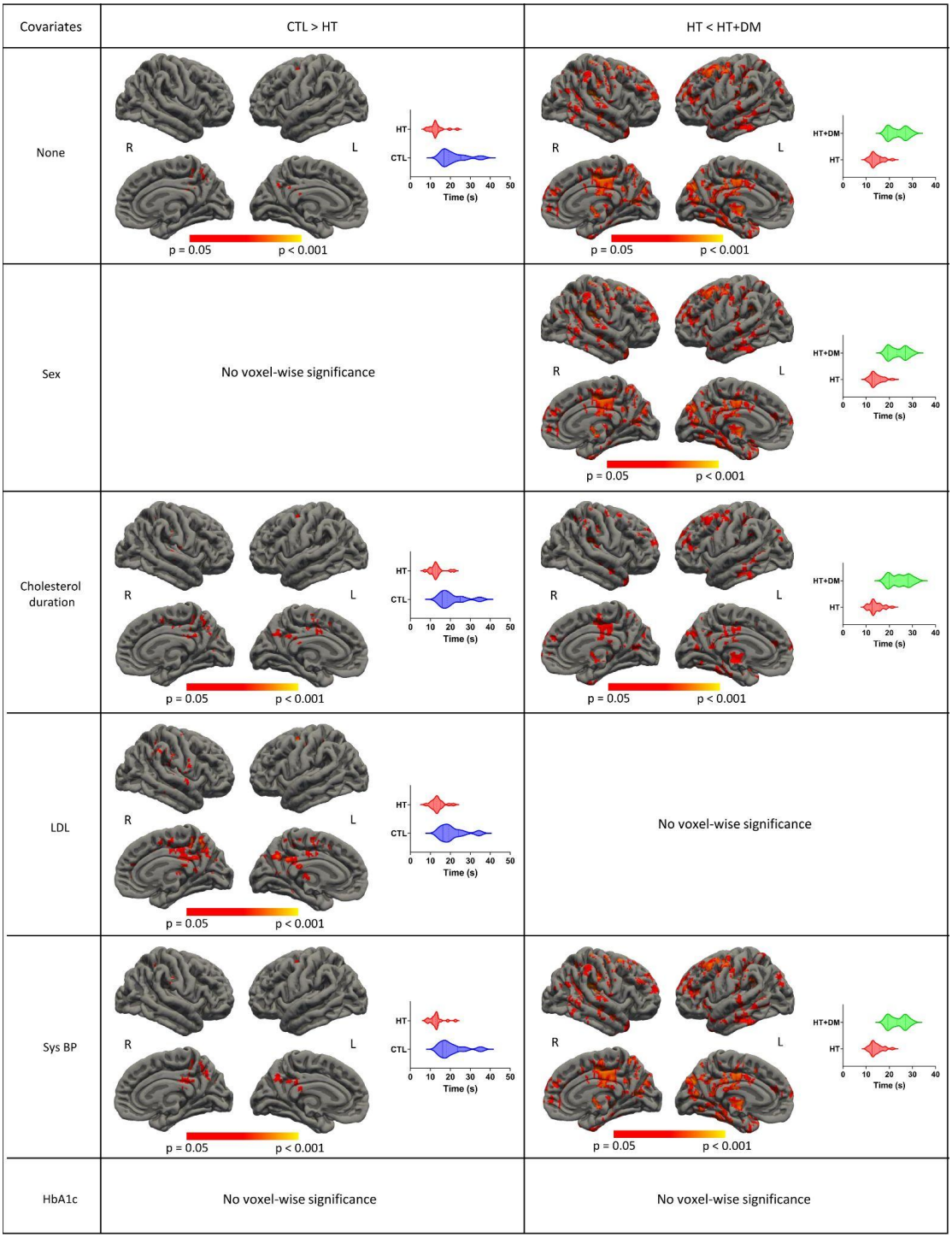

Figure 7. Voxelwise comparisons of CVR time delay. The statistical testing on the CVR time delay of CTL > HT and HT < HT+DM showed significant voxels ($p < 0.05$) for permutation inference for the general linear model after threshold-free cluster enhancement. More significant differences were detected for HT < HT+DM than CTL > HT; those were reduced when controlling for the duration of previously detected hypercholesterolemia and disappeared when controlling for LDL and HbA1c. Significant differences in CVR time delay were not detected between CTL and HT+DM.

Figure 7 shows voxels that demonstrate statistically significant differences ($p < 0.05$) where CVR time delays in CTL > HT and HT < HT+DM. More significant differences were detected for HT < HT+DM than CTL > HT and those differences were reduced when controlling for the duration of previously detected hypercholesterolemia and disappeared when controlling for LDL and HbA1c. Significant differences in CVR time delay were not detected between CTL and HT+DM.

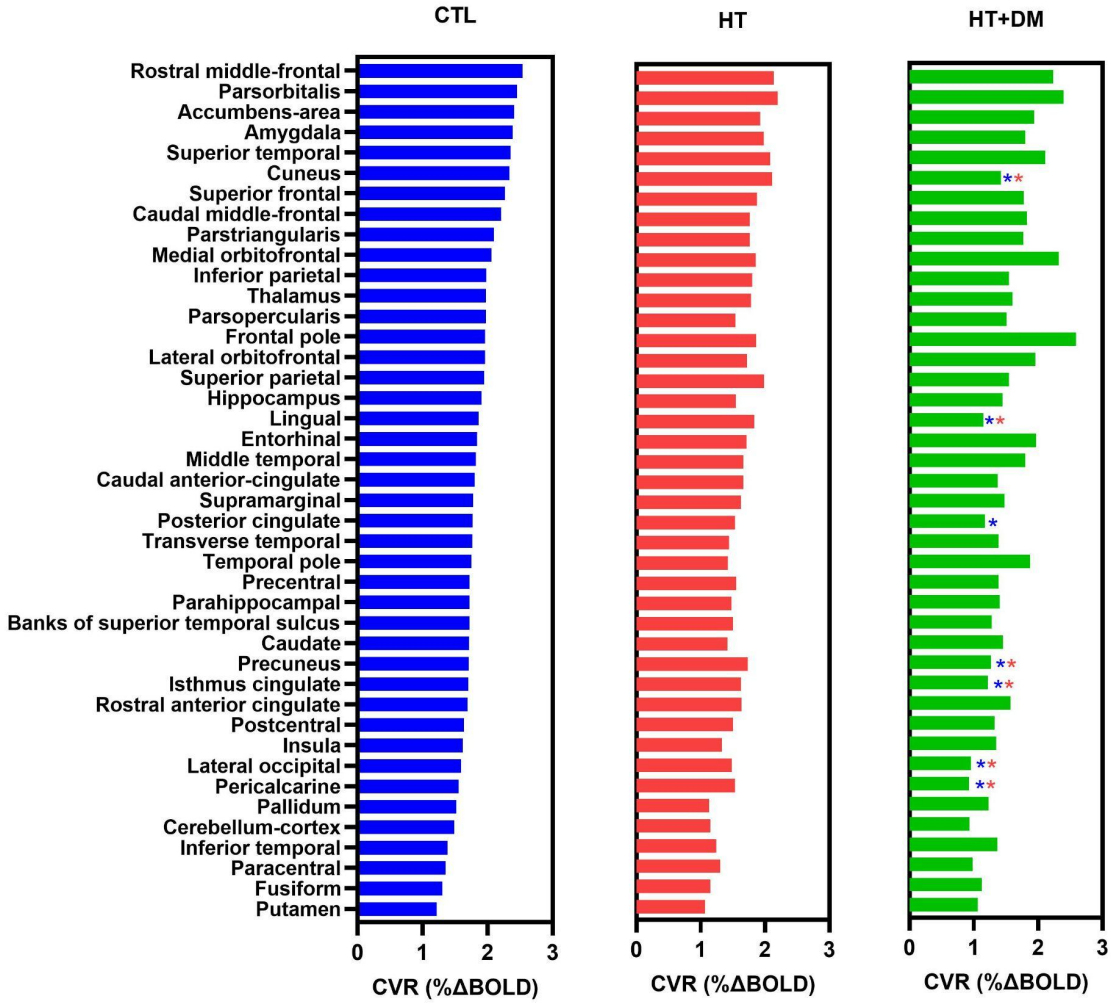

Figure 8. Mean regional CVR amplitude arranged in the descending order of CTL in subregions of the cortex. CTL showed the highest amplitude and HT+DM showed the lowest with a few exceptions. HT+DM showed statistically significant lower CVR amplitudes ($p < 0.05$) in multiple cortical regions from both CTL and HT with the Kruskal-Wallis test corrected for multiple comparisons by controlling the false discovery rate as marked by blue (*) and red (*) asterisks, respectively.

Figure 8 shows the regional means of CVR amplitude for each cortical ROI. CVR amplitude in HT+DM is significantly lower than both CTL and HT in the cuneus, the lingual, the precuneus, the isthmus cingulate, the lateral occipital, the pericalcarine, and significantly lower than CTL in the posterior cingulate.

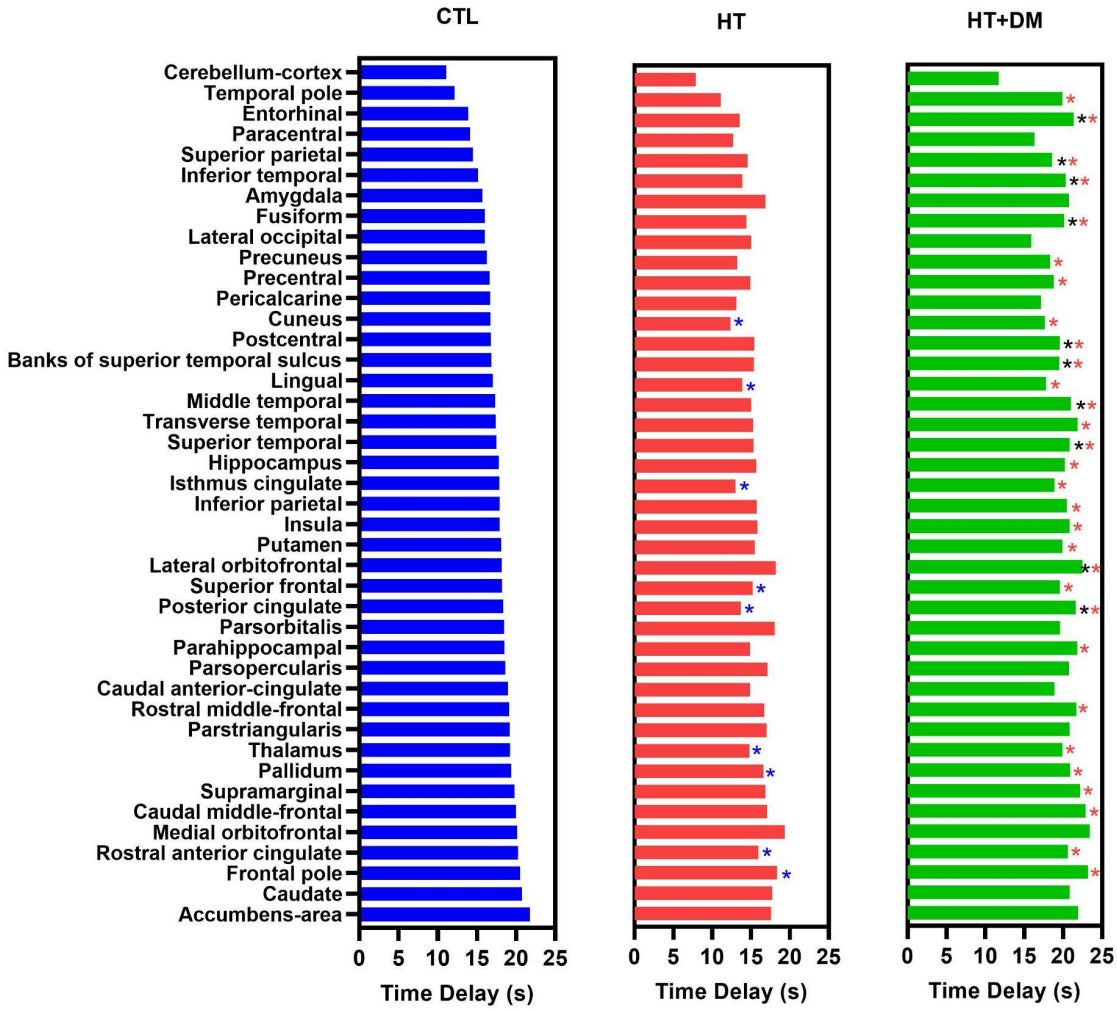

Figure 9. Mean regional CVR time delay arranged in the ascending order of CTL in subregions of the cortex. HT group showed the fastest CVR response and HT+DM showed the slowest. The CVR time delay showed statistically significant differences in more regions than those for amplitude with the Kruskal-Wallis test corrected for multiple comparisons by controlling the false discovery rate. Statistically significant shorter CVR time delay compared to CTL is marked with blue (*) and longer CVR time delays compared to CTL and HT are marked by black (*) and red (*) asterisks, respectively.

Figure 9 shows the regional means of CVR time delay for each cortical ROI. HT exhibited significantly shorter delays than CTL in the cuneus, the lingual, the isthmus cingulate, the superior frontal, the posterior cingulate, the thalamus, the pallidum, the rostral anterior cingulate, and the frontal pole. The

CVR time delay was significantly longer in HT+DM than in both CTL and HT in the entorhinal, the superior parietal, the inferior temporal, the fusiform, the postcentral, the banks of the superior temporal sulcus, the middle temporal, the superior temporal, the lateral orbitofrontal, and the posterior cingulate. HT+DM also showed a significantly longer CVR time delay in many regions compared to HT.

4. Discussion

In this work, we present a simple, frequency-domain-based, data-driven approach for estimating CVR from BH fMRI data. Our adaptive, data-driven approach for CVR estimation helps to prevent errors due to subject non-compliance and regional CVR time delay variability. It thus can have a wide range of applications in studying patient populations. Moreover, our Fourier-spectrum approach provides an elegant means to estimate voxelwise CVR time delay estimations using phase differences relative to any non-neural biological signal that depends on the BH task [Blockley et al., 2011; Pinto et al., 2020]. We demonstrate our method in the study of diabetes and hypertension.

4.1. Estimation and interpretation of CVR amplitude using BH

A BH task is a simple method to induce cerebrovascular response due to an increase of arterial CO_2 levels by ceasing ventilation. It provides a reproducible technique estimation of CVR even in less cooperative populations [Bright et al., 2009; Lipp et al., 2015; Peng et al., 2020]. The BH-induced CVR has been shown to be comparable to CVR estimated with inhaled CO_2 challenges [Chan et al., 2020; Kastrup et al., 2001; Prakash et al., 2014; Raut et al., 2016]. Model-driven approaches, mainly the general linear model (GLM), are being used for estimating CVR from BOLD data acquired during BH tasks. A function describing the block design of the breathing paradigms convolved with the hemodynamic response function is typically used to build these models of the BH CVR response [Biswal et al., 2007; Kastrup et al., 1999]. The GLM models perform well when $PETCO_2$ recordings are available for modelling BOLD response to accommodate for inter- and intra-subject variations [Bright and Murphy, 2013; Pinto et al., 2016]. However, the performance of GLM methods on data from non-compliant subjects is questionable [Jahanian et al., 2017]. The BOLD fMRI signal changes due to head motion, confounding physiological fluctuations, and other sources of noise can affect the CVR estimation from BH BOLD data [Chen et al., 2021; Jorge et al., 2013; Moia et al., 2021]. Head motion can be particularly problematic in BH CVR estimation [Johnstone et al., 2006; Moia et al., 2021]. The data affected by extensive head motion were excluded from this study instead of using complex motion correction algorithms while using the standard motion correction algorithms for correcting smaller motions. Respiration can also disturb the B0 field due to the change of air in the lungs [Raj et al., 2001] and introduce aliasing artefacts or pseudo-movement effects in the signal [Pais-Roldán et al., 2018; Power et al., 2019]. Such effects can easily result in vulnerability of the BH data analysis approach.

Alternatively, Fourier basis modelling has been used effectively, assuming sinusoidal signal variations at the paradigm design frequency [Bright and Murphy, 2013; Murphy et al., 2011; Pinto et al., 2016]. Fourier-based approaches have been reported as being robust and versatile, but are seemingly more ideal for BH designs that are symmetrical. In practice, the BOLD response to BH tasks can easily deviate from the sinusoidal frequency, and it is unclear what the implications are for CVR estimation.

In our data-driven approach, we addressed this issue by estimating fundamental frequency from the BOLD signal spectrum for accurate sinusoidal approximation of CVR. GM regions in the cortex generally have a higher CVR amplitude (**Fig. 4**) than the WM and other areas of the brain. Regional variations within the GM are also visible. Frontal regions generally have a higher CVR amplitude compared to temporal regions, the cerebellum cortex, the fusiform, and the putamen. These overall and regional differences are consistent with previous similar studies [DuBose et al., 2022; Moia et al., 2021; Thrippleton et al., 2018], and attest to the robustness of our simple approach.

4.2. CVR amplitude in diabetes and hypertension

Cerebrovascular reactivity (CVR) changes have been reported in various chronic conditions [Atwi et al., 2019; Geranmayeh et al., 2015; Iranmahboob et al., 2016; Ivankovic et al., 2013; Li et al., 2021; Yazdani et al., 2020]. Chronic hypertension [Harvey et al., 2015] has been associated with CVR impairments [Ivankovic et al., 2013; Kadoi et al., 2003; Li et al., 2021; Petrica et al., 2007; Yazdani et al., 2020]. Specifically, in HT, hypercapnia-based BOLD MRI uncovered extensive reductions in blood flow and CVR in hypertensive rats compared to controls [Li et al., 2021]. In older adults, HT is well known to be associated with arterial stiffness and blood-flow reduction [Tomoto et al., 2023] in addition to reductions in whole-brain CVR [Jefferson et al., 2018]. This CVR reduction is consistent with reduced resting-state fMRI signal fluctuations in the presence of arterial stiffness, predominantly in the precuneus, anterior and posterior cingulate gyrus, paracingulate gyrus, and frontal-pole regions [Hussein et al., 2020]. The reduced CVR is in turn associated with impaired executive function [Hajjar et al., 2014], and can be attributed to shear stress on the endothelial membrane that contributes to atherosclerosis [Webb and Werring, 2022]. Such chronic microvascular injuries also promote the spread of inflammatory factors through damaged blood-brain barriers as a potential mechanism of HT-associated neurodegeneration [Youwakim and Girouard, 2021]. In the current study, however, CVR amplitude was not significantly altered in the HT group. This can be attributed to the modest sample size and potentially high variability amongst HT individuals. This may also speak to the possibility that CVR amplitude is not the most sensitive CVR marker for HT pathology. There is minimal evidence of sex differences in the CVR impairment.

Diabetes mellitus (DM) and HT are commonly comorbid, and vascular dysfunction has long been known as a part of DM pathology. Thickening of the vascular membrane has been identified as one of the hallmarks of DM, associated with reduced vascular elasticity [Feener and King, 1997; Giordani et al., 2014]. Using transcranial Doppler ultrasound (TCD), CO_2-based CVR in the middle-cerebral artery was found to be impaired in DM [Kadoi et al., 2003]. However, studies of the effect of DM on CVR in human populations are still scarce. Ivankovic reported TCD-based vascular reactivity reductions [Ivankovic et al., 2013], echoing findings in the rat model. One of the few human MRI studies of DM+HT used the BH challenge to localize the CVR deficit to the occipital lobe [Tchistiakova et al., 2014]. Like HT, DM is also associated with blood-flow impairment [An et al., 2018; Jansen et al., 2016] as well as psychological symptoms, such as depression [Jansen et al., 2016]. Damage of the proximal tubule, involved in the uptake of vascular endothelial growth factor (VEGF) [Petrica et al., 2014], as well as a reduction in the brain-derived neurotrophic factor (BDNF) [Zhen et al., 2013], have been implicated in vascular and cognitive pathologies in DM, respectively. VEGF and BDNF are heavily involved in promoting neuronal survival through neurogenesis and angiogenesis, respectively. In the current study, CVR amplitude was found to be significantly reduced in the frontal, precuneus, posterior-cingulate and pericalcarine regions **(Fig. 6)**. To our best knowledge, this is the most extensive and detailed list of brain regions to be reported in association with CVR in DM, and these findings are consistent with regions previously reported to exhibit CVR impairment in HT [Hussein et al., 2020] and DM [Tchistiakova et al., 2014], reflecting the comorbidity in this DM+HT group. The implicated regions are known to exhibit high rates of metabolism [Raichle et al., 2001] and consequently, high blood flow [Chen et al., 2011], rendering them more susceptible to vascular damage. Like in the case of HT, there is minimal evidence of sex differences in the CVR impairment.

4.3. Estimation and interpretation of CVR delay

CVR timing has been receiving increasing attention as a marker for detecting vascular abnormalities [Donahue et al., 2015; Leung et al., 2016; Sam et al., 2016; Stickland et al., 2021; Thomas et al., 2014; Thrippleton et al., 2018] Using inspired CO_2 challenges, Leung et al. uncovered longer CVR delays in sickle-cell disease [Leung et al., 2016]. Furthermore, Holmes et al. demonstrated extended CVR delay as a marker with superior sensitivity to the effects of age and Alzheimer's disease, even when compared to the long-established CVR amplitude measures [Holmes et al., 2020].

In past literature, the BOLD temporal-lag structure has also been estimated in the resting-state BOLD signal by regressing the low-frequency (~0.1 Hz) arterial BOLD signal [Tong and Frederick, 2014], venous BOLD signal [Christen et al., 2015; Tong et al., 2018] or global BOLD signal [Amemiya et al., 2020; Mitra et al., 2014]. It is understood that the BOLD signal is an indirect measure of blood traversal, as it reflects

variations in both blood volume and blood oxygenation. Moreover, the use of the resting-state global signal as a vascular regressor is not entirely supported in concept or by experimental evidence [Scholvinck et al., 2010], and the arterial signal is not always available due to acquisition coverage limitations, for instance. An alternative is to track the BOLD signal change during a hyperoxic or hypercapnic hyperoxic (i.e. carbogen) gas challenge [Yao et al., 2021]. This latter alternative is easier to administer clinically than blood tagging while eliciting a generally robust BOLD response [Donahue et al., 2015]. Indeed, CVR-delay estimation is more robust when performed for a respiratory challenge than using resting-state data [Gong et al., 2023; Stickland et al., 2021; Zvolanek et al., 2023].

The BH task has previously been used for CVR-delay mapping [Aso et al., 2017; Geranmayeh et al., 2015; Moia et al., 2021]. Moreover, the use of Fourier analysis to elegantly estimate the BOLD-CO_2 response lag time was previously proposed with the use of a sinusoidal CO_2 stimulus [Blockley et al., 2011]. It was noted that head motion could negatively affect the accuracy of time-lag estimation using BH BOLD fMRI. Moia et al. demonstrated the advantage of using independent component analysis on multi-echo BOLD data to derive a motion-minimized model-independent BH regressor for CVR estimation [Moia et al., 2021]. The delay times are most commonly estimated as the time shift corresponding to the maximum cross-correlation or most significant linear regression in a GLM between the reference and the BOLD signals, with the reference signal being: (1) the $PETCO_2$ recording, (2) the whole-grey-matter (GM) BOLD signal [Niftrik et al., 2016; Tong and Frederick, 2014], and (3) the respiratory variability signal (RVT) [Zvolanek et al., 2023].

In our approach, the CVR delay is estimated from the phase of the filtered BOLD signal spectrum and is equivalent to the time shift mentioned earlier. However, unlike GLM-based approaches, no response model is required in our approach. Moreover, consistent with previous work demonstrating the advantages of voxel-wise sinusoidal BOLD response frequency and phase adjustments [Niftrik et al., 2016], our data-driven Fourier-domain pipeline was able to achieve robust CVR delay estimates. Pinto et al. added higher-frequency harmonics to the original single-frequency sinusoidal regressor and demonstrated improvements in CVR model fits [Pinto et al., 2016]. Equivalently, if needed, our method could easily incorporate the phases of higher-frequency spectral peaks in the delay calculation. Our chosen reference is the respiratory-belt signal, which is largely driven by BH-related variations. This is not equivalent to the RVT reference, which is based on lower-frequency respiratory variations. Our estimated delay embodies not only the transit for the CO_2 bolus to reach the brain region of interest but also the inherent time-to-peak delay of the CO_2 response function. The former reflects both systemic blood-flow velocity and transit through the main cerebrovascular arteries, while the latter reflects localized vascular elasticity. It is unfortunately not possible to separate these two quantities unless a deconvolution is performed, presenting its own technical challenges [Atwi et al., 2019; Shams et al., 2022]. The chief alternative reference signal, in the absence of the respiration belt recordings, is the whole-grey-matter

BOLD signal [Zvolanek et al., 2023], especially as the global BOLD signal variations during a BH task is largely driven by breathing. The main advantage of the GM-BOLD signal is that no external monitoring equipment is required.

In our work, CVR delay in healthy adults spans the range of 10 - 20 s in the GM. Frontal cortical regions and deep-grey regions exhibit the longest CVR delays, while the temporal and parietal regions tend to exhibit shorter delays. These observations are consistent with the work of Trippleton et al. in which the longest GM CVR delays are in the thalamus and the posterior cortex [Thrippleton et al., 2018]. However, while many publications show maps of CVR delay, few quantify regional differences, limiting our ability for cross-validation. The observed spatial diversity in CVR delay may in part be driven by differences in flow patterns in various cerebrovascular territories, including flow transit time and dispersion among others. The temporal and frontal regions, for instance, are supplied by different arterial offshoots, and borrowing from the arterial-spin labelling literature, arterial transit time from the base of the brain is thought to be longest in the occipital region and shortest in deep GM, with flow dispersion following a similar pattern [Gallichan and Jezzard, 2008]. Thus, we are led to think that vascular anatomy is not the main driver of these regional delay differences, but rather, CVR delay is driven by regional vascular elasticity. This supports the utility of CVR delays as potential early indicators of regional physiological integrity.

Of course, the respiratory-belt reference and $PETCO_2$ are not fully synchronized. For instance, we used BH upon exhale, and an increase in the belt signal corresponds to the inhale following the BH. In the period immediately after the exhale, CO_2 slowly begins to accumulate intravascularly over the 15 s BH period. Exhaled CO_2 variations in turn lag the BH pattern by approximately 15 s, with the PETCO2 value being measured only at the end of the expiratory plateau, which extends over a 4-6 s period. Thus, our respiratory-belt based CVR delay times are likely much longer than those estimated using $PETCO_2$ traces. Nonetheless, the advantages of the respiratory belt are apparent when the quality of $PETCO_2$ recordings is insufficient, which can often be the case [Zvolanek et al., 2023]. Moreover, for $PETCO_2$ recording, the need for extra equipment and often insertion of a nasal cannula, with a stipulation to breathe through the nose or through a facial mask can render participants uncomfortable.

4.4. CVR time lag in diabetes and hypertension

DM is well associated with reduced systemic [Rendell et al., 1989] and cerebral blood flow velocity [Jansen et al., 2016; Novak et al., 2006]. Reports of CVR amplitude deficits have implicated the bilateral occipito-parietal regions [Tchistiakova et al., 2014]. In this work, the main DM-related finding is that CVR delay is a more sensitive marker of diabetes than CVR amplitude, as DM+HT participants exhibited longer CVR delays in more extensive GM regions (**Fig. 9**), and delay is associated with more variables than amplitude (**Fig. 7**). The lengthened CVR delay can in part be attributed to the reduced systemic

blood-flow velocity, such as associated with vascular stiffness [Jefferson et al., 2018]. Regional cerebrovascular damage due to such factors as hyperglycemia [Giordani et al., 2014] may also stem from the reduction of the blood-derived neurotropic factor [Zhen et al., 2013], further impairing endothelial repair and survival [Kermani and Hempstead, 2019] in what is potentially a vicious cycle. Such mechanisms of endothelial dysfunction may well lead to regionally dependent CVR-response slowing akin to those of other processes such as Alzheimer's disease and aging [Peng et al., 2018]. The greater sensitivity of CVR delay than CVR amplitude for detecting the association with disease severity and patient cohort effects may suggest that the timing of a preserved CVR response is more clinically significant than the response amplitude itself.

The superior sensitivity of CVR delay to pathology extended to the HT group. One striking finding in this work is that the CVR delay time is generally shorter in the HT group than in either the CTL or HT+DM group, and this finding applies to a large number of ROIs. In contrast, there was no significant difference in CVR amplitude between the HT and CTL groups (**Fig. 8**), suggesting that a healthy CVR amplitude may belie early endothelial pathology [Webb and Werring, 2022] and that using CVR amplitude alone may lead to missed opportunities for understanding the cerebrovascular mechanisms of HT. While counterintuitive, the finding of reduced CVR delay in HT is consistent with prior ultrasound-based reports of increased blood-flow velocity in the presence of elevated blood pressure [Perret and Sloop, 2000]. Recent work using a spontaneous hypertensive model demonstrated an increase in reactive astrocytes and a reduction in microvascular density grew with HT duration [Li et al., 2021]. These changes may well contribute to a pathological speeding of the CVR response. Notably, hypertension is often comorbid with diabetes mellitus [Ivankovic et al., 2013]. However, it is common for diabetes patients to receive hypertension treatment, and as demonstrated in this work, the effect of DM on CVR delay in the DM+HT group surpasses that of HT alone.

4.5. Limitations

Our data-driven robust CVR approximation algorithm successfully estimates the fundamental BHF from BH BOLD data for sinusoidal modelling of CVR for BH paradigms with reasonably similar 'BH' and 'baseline' periods. However, we recognize that many studies may use highly asymmetrical BH timing paradigms that may not be accurately modelled by a sine-cosine function at the fundamental frequency. This can be easily addressed by adding harmonics into the signal as reported previously for sinusoidal modelling [Pinto et al., 2016].

Likewise, while we use a single most common frequency to characterize the CVR for each participant in this demonstrative study, we can add secondary frequencies in the CVR calculation. Nonetheless, in our own secondary analyses including 3 instead of 1 frequency peak for CVR estimation, the CVR amplitude

and timing differences between the groups remained unchanged, demonstrating the robustness of choosing a single "representative" BH CVR frequency.

Finally, our study used a limited number of participants. In particular, our quality-assurance standards resulted in a comparatively small DM+HT sample. In practice, it was challenging to meet our recruitment criteria particularly for the HT and DM+HT groups, resulting in a modest sample size. We hope to replicate and expand on our findings in future studies.

5. Conclusion

An adaptive data-driven approach is presented for estimating CVR from BH fMRI data to prevent errors due to subject non-compliance and regional CVR time delay variability. Our frequency-domain-based approach for CVR estimation ensures robustness in estimating the CVR using the BH task and serving as quality control of BH data, without the need for $PETCO_2$ recordings. The CVR amplitude is estimated in units of %ΔBOLD directly from the data-driven BHF. Serious deviations from the designed task paradigm were suppressed and thus did not bias the estimated CVR values. The voxelwise CVR time delay is also estimated relative to a meaningful non-brain reference point, such as the ventricles, or an external signal like a respiratory belt recording in this work. Our Fourier-spectrum based approach provides an elegant means to estimate CVR time delay estimations using phase differences relative to the reference signal that depends on the BH task.

Our robust data-driven CVR amplitude and time delay estimation can have a wide range of applications in studying patient populations. We demonstrated our method in the study of diabetes and hypertension. The CVR amplitude was lowest in HT+DM, and HT had a lower CVR amplitude than CTL regionally but the voxelwise comparison did not yield statistical significance. Interestingly, the CVR time delay was far more sensitive than the CVR amplitude to differences across the groups. While HT+DM seems to confer longer CVR delays, HT seems to confer shorter delays than CTL. These are the first MRI-based observations of CVR time delay differences between hypertensive-diabetes patients and healthy controls, demonstrating the feasibility of extracting CVR time delay using BH challenges and the unique clinical value of CVR time delay information.

Acknowledgements

We are grateful to the Canadian Institutes of Health Research (CIHR) for funding support.

References

Abbott DF, Opdam HI, Briellmann RS, Jackson GD (2005): Brief breath holding may confound functional magnetic resonance imaging studies. Hum Brain Mapp 24:284–290.

Alsop DC, Detre JA, Golay X, Günther M, Hendrikse J, Hernandez-Garcia L, Lu H, MacIntosh BJ, Parkes LM, Smits M, van Osch MJP, Wang DJJ, Wong EC, Zaharchuk G (2015): Recommended implementation of arterial spin-labeled perfusion MRI for clinical applications: A consensus of the ISMRM perfusion study group and the European consortium for ASL in dementia. Magn Reson Med 73:spcone–spcone.

Amemiya S, Takao H, Abe O (2020): Origin of the Time Lag Phenomenon and the Global Signal in Resting-State fMRI. Front Neurosci 14:596084.

An Y, Kang Y, Lee J, Ahn C, Kwon K, Choi C (2018): Blood flow characteristics of diabetic patients with complications detected by optical measurement. Biomed Eng Online 17:25.

Aso T, Jiang G, Urayama S-I, Fukuyama H (2017): A Resilient, Non-neuronal Source of the Spatiotemporal Lag Structure Detected by BOLD Signal-Based Blood Flow Tracking. Front Neurosci 11:256.

Atwi S, Shao H, Crane DE, da Costa L, Aviv RI, Mikulis DJ, Black SE, MacIntosh BJ (2019): BOLD-based cerebrovascular reactivity vascular transfer function isolates amplitude and timing responses to better characterize cerebral small vessel disease. NMR Biomed 32:e4064.

Balkau B, Hu G, Qiao Q, Tuomilehto J, Borch-Johnsen K, Pyörälä K, DECODE Study Group, European Diabetes Epidemiology Group (2004): Prediction of the risk of cardiovascular mortality using a score that includes glucose as a risk factor. The DECODE Study. Diabetologia 47:2118–2128.

Birn RM, Smith MA, Jones TB, Bandettini PA (2008): The respiration response function: the temporal dynamics of fMRI signal fluctuations related to changes in respiration. Neuroimage 40:644–654.

Biswal BB, Kannurpatti SS, Rypma B (2007): Hemodynamic scaling of fMRI-BOLD signal: validation of low-frequency spectral amplitude as a scalability factor. Magn Reson Imaging 25:1358–1369.

Blockley NP, Driver ID, Francis ST, Fisher JA, Gowland PA (2011): An improved method for acquiring cerebrovascular reactivity maps. Magn Reson Med 65:1278–1286.

Bright MG, Bulte DP, Jezzard P, Duyn JH (2009): Characterization of regional heterogeneity in cerebrovascular reactivity dynamics using novel hypocapnia task and BOLD fMRI. Neuroimage 48:166–175.

Bright MG, Murphy K (2013): Reliable quantification of BOLD fMRI cerebrovascular reactivity despite poor breath-hold performance. Neuroimage 83:559–568.

Chang C, Thomason ME, Glover GH (2008): Mapping and correction of vascular hemodynamic latency in the BOLD signal. Neuroimage 43:90–102.

Chan S-T, Evans KC, Song T-Y, Selb J, van der Kouwe A, Rosen BR, Zheng Y-P, Ahn A, Kwong KK (2020): Cerebrovascular reactivity assessment with O2-CO2 exchange ratio under brief breath hold challenge. PLoS One 15:e0225915.

Chen JJ, Pike GB (2010): Global cerebral oxidative metabolism during hypercapnia and hypocapnia in humans: implications for BOLD fMRI. J Cereb Blood Flow Metab 30:1094–1099.

Chen JJ, Rosas HD, Salat DH (2011): Age-associated reductions in cerebral blood flow are independent from regional atrophy. Neuroimage 55:468–478.

Chen K, Yang H, Zhang H, Meng C, Becker B, Biswal B (2021): Altered cerebrovascular reactivity due to respiratory rate and breath holding: a BOLD-fMRI study on healthy adults. Brain Struct Funct 226:1229–1239.

Christen T, Jahanian H, Ni WW, Qiu D, Moseley ME, Zaharchuk G (2015): Noncontrast mapping of arterial delay and functional connectivity using resting-state functional MRI: a study in Moyamoya patients. J Magn Reson Imaging 41:424–430.

Cox RW (1996): AFNI: software for analysis and visualization of functional magnetic resonance neuroimages. Comput Biomed Res 29:162–173.

Cox RW, Hyde JS (1997): Software tools for analysis and visualization of fMRI data. NMR Biomed 10:171–178.

D'Agostino RB, Stephens M (1986): Tests for normal distribution in goodness-of-fit techniques. Marcel Decker.

Dlamini N, Shah-Basak P, Leung J, Kirkham F, Shroff M, Kassner A, Robertson A, Dirks P, Westmacott R, deVeber G, Logan W (2018): Breath-Hold Blood Oxygen Level-Dependent MRI: A Tool for the Assessment of Cerebrovascular Reserve in Children with Moyamoya Disease. AJNR Am J Neuroradiol 39:1717–1723.

Donahue MJ, Strother MK, Lindsey KP, Hocke LM, Tong Y, Frederick BD (2015): Time delay processing of hypercapnic fMRI allows quantitative parameterization of cerebrovascular reactivity and blood flow delays. J Cereb Blood Flow Metab 36:1767–1779.

DuBose LE, Weng TB, Pierce GL, Wharff C, Reist L, Hamilton C, O'Deen A, Dubishar K, Lane-Cordova A, Voss MW (2022): Association between cardiorespiratory fitness and cerebrovascular reactivity to a breath-hold stimulus in older adults: influence of aerobic exercise training. J Appl Physiol 132:1468–1479.

Feener EP, King GL (1997): Vascular dysfunction in diabetes mellitus. Lancet 350 Suppl 1:SI9–13.

Gallichan D, Jezzard P (2008): Modeling the effects of dispersion and pulsatility of blood flow in pulsed arterial spin labeling. Magn Reson Med 60:53–63.

Geranmayeh F, Wise RJS, Leech R, Murphy K (2015): Measuring vascular reactivity with breath-holds after stroke: a method to aid interpretation of group-level BOLD signal changes in longitudinal fMRI studies. Hum Brain Mapp 36:1755–1771.

Giordani I, Di Flaviani A, Picconi F, Malandrucco I, Ylli D, Palazzo P, Altavilla R, Vernieri F, Passarelli F, Donno S, Lauro D, Pasqualetti P, Frontoni S (2014): Acute hyperglycemia reduces cerebrovascular reactivity: the role of glycemic variability. J Clin Endocrinol Metab 99:2854–2860.

Gong J, Stickland RC, Bright MG (2023): Hemodynamic timing in resting-state and breathing-task BOLD fMRI. bioRxiv. https://www.biorxiv.org/content/10.1101/2022.11.11.516194.

Haight TJ, Bryan RN, Erus G, Davatzikos C, Jacobs DR, D'Esposito M, Lewis CE, Launer LJ (2015): Vascular risk factors, cerebrovascular reactivity, and the default-mode brain network. Neuroimage 115:7–16.

Hajjar I, Marmerelis V, Shin DC, Chui H (2014): Assessment of Cerebrovascular Reactivity during Resting State Breathing and Its Correlation with Cognitive Function in Hypertension. Cerebrovasc Dis 38:10–16.

Halani S, Kwinta JB, Golestani AM, Khatamian YB, Chen JJ (2015): Comparing cerebrovascular reactivity measured using BOLD and cerebral blood flow MRI: The effect of basal vascular tension on vasodilatory and vasoconstrictive reactivity. Neuroimage 110:110–123.

Harvey A, Montezano AC, Touyz RM (2015): Vascular biology of ageing-Implications in hypertension. J Mol Cell Cardiol 83:112–121.

Hauser T-K, Seeger A, Bender B, Klose U, Thurow J, Ernemann U, Tatagiba M, Meyer PT, Khan N, Roder C (2019): Hypercapnic BOLD MRI compared to H215O PET/CT for the hemodynamic evaluation of patients with Moyamoya Disease. Neuroimage Clin 22:101713.

Heijtel DFR, Mutsaerts HJMM, Bakker E, Schober P, Stevens MF, Petersen ET, van Berckel BNM, Majoie CBLM, Booij J, van Osch MJP, Vanbavel E, Boellaard R, Lammertsma AA, Nederveen AJ (2014): Accuracy and precision of pseudo-continuous arterial spin labeling perfusion during baseline and hypercapnia: a head-to-head comparison with ^{15}O H_2O positron emission tomography. Neuroimage 92:182–192.

Holmes KR, Tang-Wai D, Sam K, McKetton L, Poublanc J, Crawley AP, Sobczyk O, Cohn M, Duffin J, Tartaglia MC, Black SE, Fisher JA, Wasserman B, Mikulis DJ (2020): Slowed Temporal and Parietal Cerebrovascular Response in Patients with Alzheimer's Disease. Can J Neurol Sci 47:366–373.

Hussein A, Matthews JL, Syme C, Macgowan C, MacIntosh BJ, Shirzadi Z, Pausova Z, Paus T, Chen JJ (2020): The association between resting-state functional magnetic resonance imaging and aortic pulse-wave velocity in healthy adults. Hum Brain Mapp. http://dx.doi.org/10.1002/hbm.24934.

Iranmahboob A, Peck KK, Brennan NP, Karimi S, Fisicaro R, Hou B, Holodny AI (2016): Vascular Reactivity Maps in Patients with Gliomas Using Breath-Holding BOLD fMRI. J Neuroimaging 26:232–239.

Ivankovic M, Radman M, Gverovic-Antunica A, Tesanovic S, Trgo G, Demarin V (2013): Influence of hypertension and type 2 diabetes mellitus on cerebrovascular reactivity in diabetics with retinopathy. Ann Saudi Med 33:130–133.

Jahanian H, Christen T, Moseley ME, Pajewski NM, Wright CB, Tamura MK, Zaharchuk G, SPRINT Study Research Group (2017): Measuring vascular reactivity with resting-state blood oxygenation level-dependent (BOLD) signal fluctuations: A potential alternative to the breath-holding challenge? J Cereb Blood Flow Metab 37:2526–2538.

Jansen JFA, van Bussel FCG, van de Haar HJ, van Osch MJP, Hofman PAM, van Boxtel MPJ, van Oostenbrugge RJ, Schram MT, Stehouwer CDA, Wildberger JE, Backes WH (2016): Cerebral blood flow, blood supply, and cognition in Type 2 Diabetes Mellitus. Sci Rep 6:1–9.

Jefferson AL, Cambronero FE, Liu D, Moore EE, Neal JE, Terry JG, Nair S, Pechman KR, Rane S, Davis LT, Gifford KA, Hohman TJ, Bell SP, Wang TJ, Beckman JA, Carr JJ (2018): Higher Aortic Stiffness is

Related to Lower Cerebral Blood Flow and Preserved Cerebrovascular Reactivity in Older Adults. Circulation. http://dx.doi.org/10.1161/CIRCULATIONAHA.118.032410.

Jenkinson M, Beckmann CF, Behrens TEJ, Woolrich MW, Smith SM (2012): FSL. Neuroimage 62:782–790.

Johnstone T, Ores Walsh KS, Greischar LL, Alexander AL, Fox AS, Davidson RJ, Oakes TR (2006): Motion correction and the use of motion covariates in multiple-subject fMRI analysis. Hum Brain Mapp 27:779–788.

Jorge J, Figueiredo P, van der Zwaag W, Marques JP (2013): Signal fluctuations in fMRI data acquired with 2D-EPI and 3D-EPI at 7 Tesla. Magn Reson Imaging 31:212–220.

Kadoi Y, Hinohara H, Kunimoto F, Saito S, Ide M, Hiraoka H, Kawahara F, Goto F (2003): Diabetic patients have an impaired cerebral vasodilatory response to hypercapnia under propofol anesthesia. Stroke 34:2399–2403.

Kannurpatti SS, Biswal BB (2008): Detection and scaling of task-induced fMRI-BOLD response using resting state fluctuations. Neuroimage 40:1567–1574.

Kastrup A, Krüger G, Neumann-Haefelin T, Moseley ME (2001): Assessment of cerebrovascular reactivity with functional magnetic resonance imaging: comparison of CO(2) and breath holding. Magn Reson Imaging 19:13–20.

Kastrup A, Li TQ, Glover GH, Moseley ME (1999): Cerebral blood flow-related signal changes during breath-holding. AJNR Am J Neuroradiol 20:1233–1238.

Kermani P, Hempstead B (2019): BDNF Actions in the Cardiovascular System: Roles in Development, Adulthood and Response to Injury. Front Physiol 10:455.

Kleiser B, Widder B (1992): Course of carotid artery occlusions with impaired cerebrovascular reactivity. Stroke 23:171–174.

Leung J, Duffin J, Fisher JA, Kassner A (2016): MRI-based cerebrovascular reactivity using transfer function analysis reveals temporal group differences between patients with sickle cell disease and healthy controls. NeuroImage: Clinical 12:624–630.

Lipp I, Murphy K, Caseras X, Wise RG (2015): Agreement and repeatability of vascular reactivity estimates based on a breath-hold task and a resting state scan. Neuroimage 113:387–396.

Liu H-L, Huang JU-C, Wu C-T, Hsu Y-Y (2002): Detectability of blood oxygenation level-dependent signal changes during short breath hold duration. Magn Reson Imaging 20:643–648.

Liu P, Liu G, Pinho MC, Lin Z, Thomas BP, Rundle M, Park DC, Huang J, Welch BG, Lu H (2021): Cerebrovascular Reactivity Mapping Using Resting-State BOLD Functional MRI in Healthy Adults and Patients with Moyamoya Disease. Radiology 299:419–425.

Liu P, Li Y, Pinho M, Park DC, Welch BG, Lu H (2017a): Cerebrovascular reactivity mapping without gas challenges. Neuroimage 146:320–326.

Liu P, Welch BG, Li Y, Gu H, King D, Yang Y, Pinho M, Lu H (2017b): Multiparametric imaging of brain hemodynamics and function using gas-inhalation MRI. Neuroimage 146:715–723.

Li Y, Li R, Liu M, Nie Z, Muir ER, Duong TQ (2021): MRI study of cerebral blood flow, vascular reactivity, and vascular coupling in systemic hypertension. Brain Res 1753:147224.

Magon S, Basso G, Farace P, Ricciardi GK, Beltramello A, Sbarbati A (2009): Reproducibility of BOLD signal change induced by breath holding. Neuroimage 45:702–712.

Mandell DM, Han JS, Poublanc J, Crawley AP, Stainsby JA, Fisher JA, Mikulis DJ (2008): Mapping cerebrovascular reactivity using blood oxygen level-dependent MRI in Patients with arterial steno-occlusive disease: comparison with arterial spin labeling MRI. Stroke 39:2021–2028.

Mark CI, Slessarev M, Ito S, Han J, Fisher JA, Pike GB (2010): Precise control of end-tidal carbon dioxide and oxygen improves BOLD and ASL cerebrovascular reactivity measures. Magn Reson Med 64:749–756.

Mitra A, Snyder AZ, Hacker CD, Raichle ME (2014): Lag structure in resting-state fMRI. J Neurophysiol 111:2374–2391.

Moia S, Termenon M, Uruñuela E, Chen G, Stickland RC, Bright MG, Caballero-Gaudes C (2021): ICA-based denoising strategies in breath-hold induced cerebrovascular reactivity mapping with multi echo BOLD fMRI. Neuroimage 233:117914.

Murphy K, Harris AD, Wise RG (2011): Robustly measuring vascular reactivity differences with breath-hold: normalising stimulus-evoked and resting state BOLD fMRI data. Neuroimage 54:369–379.

Niftrik CHB, Piccirelli M, Bozinov O, Pangalu A, Valavanis A, Regli L, Fierstra J (2016): Fine tuning breath-hold-based cerebrovascular reactivity analysis models. Brain Behav 6. https://onlinelibrary.wiley.com/doi/10.1002/brb3.426.

Novak V, Last D, Alsop DC, Abduljalil AM, Hu K, Lepicovsky L, Cavallerano J, Lipsitz LA (2006): Cerebral blood flow velocity and periventricular white matter hyperintensities in type 2 diabetes. Diabetes Care 29:1529–1534.

Ogasawara K, Ito H, Sasoh M, Okuguchi T, Kobayashi M, Yukawa H, Terasaki K, Ogawa A (2003): Quantitative measurement of regional cerebrovascular reactivity to acetazolamide using 123I-N-isopropyl-p-iodoamphetamine autoradiography with SPECT: validation study using H2 15O with PET. J Nucl Med 44:520–525.

Pais-Roldán P, Biswal B, Scheffler K, Yu X (2018): Identifying Respiration-Related Aliasing Artifacts in the Rodent Resting-State fMRI. Front Neurosci 12:788.

Peng S-L, Chen X, Li Y, Rodrigue KM, Park DC, Lu H (2018): Age-related changes in cerebrovascular reactivity and their relationship to cognition: A four-year longitudinal study. Neuroimage 174:257–262.

Peng S-L, Yang H-C, Chen C-M, Shih C-T (2020): Short- and long-term reproducibility of BOLD signal change induced by breath-holding at 1.5 and 3 T. NMR Biomed 33:e4195.

Perret RS, Sloop GD (2000): Increased peak blood velocity in association with elevated blood pressure. Ultrasound Med Biol 26:1387–1391.

Petrica L, Petrica M, Vlad A, Bob F, Gluhovschi C, Gluhovschi G, Jianu CD, Ursoniu S, Schiller A, Velciov S, Trandafirescu V, Bozdog G (2007): Cerebrovascular reactivity is impaired in patients with

non-insulin-dependent diabetes mellitus and microangiopathy. Wien Klin Wochenschr 119:365–371.

Petrica L, Vlad A, Gluhovschi G, Gadalean F, Dumitrascu V, Gluhovschi C, Velciov S, Bob F, Vlad D, Popescu R, Milas O, Ursoniu S (2014): Proximal tubule dysfunction is associated with podocyte damage biomarkers nephrin and vascular endothelial growth factor in type 2 diabetes mellitus patients: a cross-sectional study. PLoS One 9:e112538.

Pinto J, Bright MG, Bulte DP, Figueiredo P (2020): Cerebrovascular Reactivity Mapping Without Gas Challenges: A Methodological Guide. Front Physiol 11:608475.

Pinto J, Jorge J, Sousa I, Vilela P, Figueiredo P (2016): Fourier modeling of the BOLD response to a breath-hold task: Optimization and reproducibility. Neuroimage 135:223–231.

Power JD, Lynch CJ, Silver BM, Dubin MJ, Martin A, Jones RM (2019): Distinctions among real and apparent respiratory motions in human fMRI data. Neuroimage 201:116041.

Prakash K, Chandran DS, Khadgawat R, Jaryal AK, Deepak KK (2014): Correction for Blood Pressure Improves Correlation between Cerebrovascular Reactivity Assessed by Breath Holding and 6% CO2 Breathing. J Stroke Cerebrovasc Dis 23:630–635.

Raichle ME, MacLeod AM, Snyder AZ, Powers WJ, Gusnard DA, Shulman GL (2001): A default mode of brain function. Proc Natl Acad Sci U S A 98:676–682.

Raj D, Anderson AW, Gore JC (2001): Respiratory effects in human functional magnetic resonance imaging due to bulk susceptibility changes. Phys Med Biol 46:3331–3340.

Raut RV, Nair VA, Sattin JA, Prabhakaran V (2016): Hypercapnic evaluation of vascular reactivity in healthy aging and acute stroke via functional MRI. Neuroimage Clin 12:173–179.

Rendell M, Bergman T, O'Donnell G, Drobny E, Borgos J, Bonner RF (1989): Microvascular blood flow, volume, and velocity measured by laser Doppler techniques in IDDM. Diabetes 38:819–824.

Sam K, Peltenburg B, Conklin J, Sobczyk O, Poublanc J, Crawley AP, Mandell DM, Venkatraghavan L, Duffin J, Fisher JA, Black SE, Mikulis DJ (2016): Cerebrovascular reactivity and white matter integrity. Neurology 87:2333–2339.

Scholvinck ML, Maier A, Ye FQ, Duyn JH, Leopold DA (2010): Neural basis of global resting-state fMRI activity. Proc Natl Acad Sci U S A 107:10238–10243.

Shams S, Prokopiou P, Esmaelbeigi A, Mitsis GD, Chen JJ (2022): Modeling the dynamics of cerebrovascular reactivity to carbon dioxide in fMRI under task and resting-state conditions. Neuroimage 265:119758.

Smith SM, Jenkinson M, Woolrich MW, Beckmann CF, Behrens TEJ, Johansen-Berg H, Bannister PR, De Luca M, Drobnjak I, Flitney DE, Niazy RK, Saunders J, Vickers J, Zhang Y, De Stefano N, Brady JM, Matthews PM (2004): Advances in functional and structural MR image analysis and implementation as FSL. Neuroimage 23 Suppl 1:S208–19.

Smith SM, Nichols TE (2009): Threshold-free cluster enhancement: addressing problems of smoothing, threshold dependence and localisation in cluster inference. Neuroimage 44:83–98.

Sousa I, Vilela P, Figueiredo P (2014): Reproducibility of hypocapnic cerebrovascular reactivity

measurements using BOLD fMRI in combination with a paced deep breathing task. Neuroimage 98:31–41.

Spano VR, Mandell DM, Poublanc J, Sam K, Battisti-Charbonney A, Pucci O, Han JS, Crawley AP, Fisher JA, Mikulis DJ (2013): CO2 blood oxygen level-dependent MR mapping of cerebrovascular reserve in a clinical population: safety, tolerability, and technical feasibility. Radiology 266:592–598.

Stickland RC, Zvolanek KM, Moia S, Ayyagari A, Caballero-Gaudes C, Bright MG (2021): A practical modification to a resting state fMRI protocol for improved characterization of cerebrovascular function. Neuroimage 239:118306.

Stringer MS, Blair GW, Shi Y, Hamilton I, Dickie DA, Doubal FN, Marshall IM, Thrippleton MJ, Wardlaw JM (2021): A Comparison of CVR Magnitude and Delay Assessed at 1.5 and 3T in Patients With Cerebral Small Vessel Disease. Front Physiol 12:644837.

Tancredi FB, Hoge RD (2013): Comparison of cerebral vascular reactivity measures obtained using breath-holding and CO2 inhalation. J Cereb Blood Flow Metab 33:1066–1074.

Tchistiakova E, Anderson ND, Greenwood CE, MacIntosh BJ (2014): Combined effects of type 2 diabetes and hypertension associated with cortical thinning and impaired cerebrovascular reactivity relative to hypertension alone in older adults. Neuroimage Clin 5:36–41.

Thomas BP, Liu P, Aslan S, King KS, van Osch MJP, Lu H (2013): Physiologic underpinnings of negative BOLD cerebrovascular reactivity in brain ventricles. Neuroimage 83:505–512.

Thomas BP, Liu P, Park DC, van Osch MJP, Lu H (2014): Cerebrovascular Reactivity in the Brain White Matter: Magnitude, Temporal Characteristics, and Age Effects. J Cereb Blood Flow Metab 34:242–247.

Thrippleton MJ, Shi Y, Blair G, Hamilton I, Waiter G, Schwarzbauer C, Pernet C, Andrews PJ, Marshall I, Doubal F, Wardlaw JM (2018): Cerebrovascular reactivity measurement in cerebral small vessel disease: Rationale and reproducibility of a protocol for MRI acquisition and image processing. Int J Stroke 13:195–206.

Tomoto T, Tarumi T, Zhang R (2023): Central arterial stiffness, brain white matter hyperintensity and total brain volume across the adult lifespan. J Hypertens. http://dx.doi.org/10.1097/HJH.0000000000003404.

Tong Y, Frederick BD (2014): Tracking cerebral blood flow in BOLD fMRI using recursively generated regressors. Hum Brain Mapp 35:5471–5485.

Tong Y, Yao JF, Chen JJ, Frederick BD (2018): The resting-state fMRI arterial signal predicts differential blood transit time through the brain. J Cereb Blood Flow Metab:271678X17753329.

Urback AL, MacIntosh BJ, Goldstein BI (2017): Cerebrovascular reactivity measured by functional magnetic resonance imaging during breath-hold challenge: A systematic review. Neurosci Biobehav Rev 79:27–47.

Urback AL, Metcalfe AWS, Korczak DJ, MacIntosh BJ, Goldstein BI (2018): Magnetic resonance imaging of cerebrovascular reactivity in healthy adolescents. J Neurosci Methods 306:1–9.

Webb AJS, Werring DJ (2022): New Insights Into Cerebrovascular Pathophysiology and Hypertension.

Stroke 53:1054–1064.

Welsh KA, Breitner JCS, Magruder-Habib KM (1993): Detection of Dementia in the Elderly Using Telephone Screening of Cognitive Status. Cogn Behav Neurol 6:103.

Wilson PW, D'Agostino RB, Levy D, Belanger AM, Silbershatz H, Kannel WB (1998): Prediction of coronary heart disease using risk factor categories. Circulation 97:1837–1847.

Winkler AM, Ridgway GR, Webster MA, Smith SM, Nichols TE (2014): Permutation inference for the general linear model. Neuroimage 92:381–397.

Wise RG, Pattinson KTS, Bulte DP, Chiarelli PA, Mayhew SD, Balanos GM, O'Connor DF, Pragnell TR, Robbins PA, Tracey I, Jezzard P (2007): Dynamic forcing of end-tidal carbon dioxide and oxygen applied to functional magnetic resonance imaging. J Cereb Blood Flow Metab 27:1521–1532.

Wu P, Bandettini PA, Harper RM, Handwerker DA (2015): Effects of thoracic pressure changes on MRI signals in the brain. J Cereb Blood Flow Metab 35:1024–1032.

Yao JF, Yang H-CS, Wang JH, Liang Z, Talavage TM, Tamer GG Jr, Jang I, Tong Y (2021): A novel method of quantifying hemodynamic delays to improve hemodynamic response, and CVR estimates in CO2 challenge fMRI. J Cereb Blood Flow Metab 41:1886–1898.

Yazdani N, Kindy MS, Taheri S (2020): CBF regulation in hypertension and Alzheimer's disease. Clin Exp Hypertens 42:622–639.

Youwakim J, Girouard H (2021): Inflammation: A Mediator Between Hypertension and Neurodegenerative Diseases. Am J Hypertens 34:1014–1030.

Zhao MY, Fan AP, Chen DY-T, Sokolska MJ, Guo J, Ishii Y, Shin DD, Khalighi MM, Holley D, Halbert K, Otte A, Williams B, Rostami T, Park J-H, Shen B, Zaharchuk G (2021): Cerebrovascular reactivity measurements using simultaneous 15O-water PET and ASL MRI: Impacts of arterial transit time, labeling efficiency, and hematocrit. Neuroimage 233:117955.

Zhen YF, Zhang J, Liu XY, Fang H, Tian LB, Zhou DH, Kosten TR, Zhang XY (2013): Low BDNF is associated with cognitive deficits in patients with type 2 diabetes. Psychopharmacology 227:93–100.

Zvolanek KM, Moia S, Dean JN, Stickland RC, Caballero-Gaudes C, Bright MG (2023): Comparing end-tidal CO2, respiration volume per time (RVT), and average gray matter signal for mapping cerebrovascular reactivity amplitude and delay with breath-hold task BOLD fMRI. Neuroimage 272:120038.